PROCEEDINGS OF SCIENCE

Protoplanetary Disks – A Review

Tomoyuki Hanawa*
Center for Frontier Science, Chiba University, 1-33 Yayoi-cho, Inage-ku, Chiba 263-8522, Japan
E-mail: hanawa@faculty.chiba-u.jp

This article reviews historical development of our understanding of protoplanetary disks. Protoplatary disks have been studied by various types of observations ranging from optical through infrared to radio emissions. The progress of our understanding deeply owes technological advances in the observations. This article reviews various methods to identify the protoplanetary disks. They include infrared color (spectral energy distribution), the Doppler shift due to rotation, imaging, and indirect evidences such as jets and outflows. It also lists up surveys useful for the study of protoplanetary disks. After several recent topics interesting the author are introduced, it is concluded with a short summary.

Accretion Processes in Cosmic Sources – APCS2016 –
5-10 September 2016,
Saint Petersburg, Russia

*Speaker.

PoS(APCS2016)009

1. Introduction

Protoplanetary disks have been interested by human beings for more than several centuries. It is the 18-th century that Emanuel Swedenborg, Immanuel Kant, and Pierre-Simon Laplace discussed the nebular hypothesis on the origin of the Solar system. However, the protoplanetary disks had been hypothetical for many years and the observations of them have been enabled by recent progress in the technology. The progress includes great improvement in angular resolution, spectral resolution, and sensitivity in all the wavelengths ranging from X-ray to radio.

This article reviews historical development in our understanding of formation and structure of the protoplanetary disks. We review the methods of identifying protoplanetary disks in §2. They are identified by the spectral energy distribution in the infrared, Doppler shifted molecular line emissions, and near infrared images showing the disk shape. Also listed are Indirect evidences suggesting the presence of a protoplanetary disk. Surveys providing census of protoplanetary disks are reviewed in §3. Recent observations and some topics are described in §4. A short summary is given in §5.

2. Era of Identification

This section describes various methods of identifying protoplanetary disks.

2.1 Color Identification

The earliest evidence for a protoplanetary disk was brought from infrared observations of young stars. The spectral energy distribution (SED) of a naked star is approximately that of a black body having the stellar radius. Hence the SED has the slope,

$$\alpha = \frac{d\ln(\lambda F_\lambda)}{d\ln\lambda} = -\frac{d\ln(\nu F_\nu)}{d\ln\nu} = -3 \tag{2.1}$$

in the infrared since the Rayleigh-Jeans approximation is valid. Here, the symbols, λ and ν, denote the wavelength and frequency, respectively, while F_λ and F_ν do the flux per unit wavelength and that per unit frequency, respectively. Protoplanetary disks shine in the infrared and hence the slope is shallower when the young stars are associated with them.

The current classification of protoplanetary disks dates back to Lada [1]. He classified embedded young stellar objects (YSOs) into three classes according to the infrared SED obtained by Lada & Wilking [2]. In his original classification scheme, class I, II, and III sources are defined as those in the range of $0 < \alpha \lesssim +3$, $-2 \lesssim \alpha \lesssim 0$, and $-3 \lesssim \alpha \lesssim -2$, respectively. The SED slope is often measured in the wavelength range between 2 and 25 μm. The roman numbers are assigned according to the theoretical expectation that YSOs evolve from class I to III, i.e., the infrared excess decreases with time. Class II sources correspond to the classical T Tauri stars while class III sources to the weak lined T Tauri stars. Later by André, Ward-Thompson & Barsony [3], this classification was extended to an earlier object, class 0 sources which have neither optical or near infrared counter part. Thus YSOs are now thought to evolve from class 0 to class III in general.

SED is a good indicator for the radial extent of the protoplanetary disk. Each radial portion of the protoplanetary disk radiate in the wavelength corresponding the temperature thereof. An outer

part of the disk is cooler and the emission therefrom is restricted in a longer wavelength. It means that the protoplanetary disks are extended in class I sources. A class of sources named transitional disks show a dip around $\lambda \simeq 10$ μm in the SED. The dip is attributed to a wide gap in the disks (see, e.g., a review by Williams & Cieza [4]).

SED depends on the viewing angle, i.e., the inclination of the disk to the line of sight. An edge-on disk may have an apparently younger SED since the inner part may be hidden from our view. It is also important to note that the SED classification does not give a unique description of the amount and distribution of circumstellar material. See, e.g., Williams & Cieza [4] and references therein for further details.

2.2 Kinematical Identification

Protoplanetary disks are supported by rotation against gravity. When the gravity is dominated by the central star, the rotation velocity is evaluated to be

$$v_\varphi = \sqrt{\frac{GM}{r}} = 2.98 \left(\frac{M}{1\,M_\odot}\right)^{1/2} \left(\frac{r}{100\ \mathrm{au}}\right)^{-1/2} \ \mathrm{km\ s^{-1}}, \tag{2.2}$$

where G, M, and r denote the gravitational constant, the mass of the star, and the radial distance from the star, respectively. An attempt to measure the rotation was initiated in 1980s.

Dutrey, Guilloteau & Simon [5] resolved a rotating disk around GG Tau in the ^{13}CO $J = 1 \to 0$ emission by using the IRAM interferometer. This is recognized as the earliest sure detection of the rotation although some earlier papers claimed detection. It should be noted that the angular resolution was $2.''6 \times 2.''0$ in their observation. This resolution corresponds to 360 au $\times$ 300 au in the linear dimension for the assumed distance 140 pc and was not enough to confirm the radial dependence of the rotation velocity expressed in equation (2.2).

The angular resolution has been progressively improved. Tang et al. [6] observed the disk around GG Tau with 50 au spatial resolution by using the radio interferometer, ALMA. The ALMA observation shows the 2D distribution of the Doppler shift in the ^{13}CO $J = 3 \to 2$ emission. The radial velocity increases from East to West and some channel maps show typical "butterfly" shape. Tang et al. [6] inferred to an embedded planet based on the distortion seen in the channel maps.

2.3 Image Identification

The disk shape was elucidated by the Hubble Space Telescope (HST) thanks to its high angular resolution of $\sim 0.''1$.

O'Dell, Wen & Hu [7] discovered the silhouettes due to protoplanetary disks in the HST image of M42 (the Orion nebula) and coined the term "ploplyds" to them. The properties of the ploplyds were examined by O'Dell & Wen [8] who observed M42 again with the HST after its postrefurbishment for the spherical aberation. Since the ploplyds are identified by absorption of the back ground emission, the column mass density of the disk can be derived with lower uncertainty. O'Dell & Wen [8] evaluated the characteristic mass of ionized material to be 2×10^{28} g.

Padgett et al. [9] observed three class I sources and three low luminosity stars associated with Herbig-Haro jets in the Taurus star forming region with the NICMOS camera on board HST. All these sources were found to have circumstellar reflection nebulae crossed by dark lanes. The dark

lanes are the protoplanetary disks in the edge-on view and the reflection nebulae correspond to the upper disk surfaces. The reflection nebulae indicate that the disks are flared up, i.e., the ratio of the height to the radius increases with the radius. The Herbig-Haro jets extend in the direction perpendicular to the dark lane, i.e., the disk, which implies that the jets emerge from the disks.

Currently high angular resolution is achieved by the large ground based telescope equipped with the adaptive optics. The H-band (1.6 μm) and K-band (2.0 μm) images of the protoplanetary disks have been taken with such large ground based telescopes. Often the central stars are masked by a corona graph. The images often show spiral and ring features in the protoplanetary disks. The origin of the features remain unknown although several ideas are proposed. See the article by Mayama in this volume for some examples.

2.4 Indirect Evidences

As shown in the previous subsection, class I sources are often associated with jets and outflows. Also class 0 sources are also known to be associated with outflows. The close association implies that jets and outflows can be regarded as indirect evidence for the protostellar disks. The disks are expected to be oriented normal to the jets and outflows.

H_α emission and X-ray emission can be regarded as an evidence for accretion in some form and hence indirect evidence for the disks as reservoir for the accretion. H_α emission and variabilities have served as indicators for YSO candidates. Also X-ray emission has been served as an indicator for the YSO candidate since the seminal work by Montmerle et al. [10]. They observed the ρ Ophiuchi dark cloud region with the Einstein Observatry and detected many weak variable sources, one half of which were already known to be YSOs at that time.

3. Era of Survey

Many class 0 sources are designated by the name which are headed by IRAS and then followed by the right ascension and declination, such as IRAS 16293$-$2422. The names indicate that these sources were discovered thorough the all sky survey with the InfraRed Astronomical Satellite (IRAS). The IRAS satellite was launched in January 1983 and detected a half million infrared sources during the 10 months operation. The infrared sources include YSOs as well as external galaxies.

Several all sky surveys have been performed successfully in these two decades.

Two Micron All-Sky Survey (2MASS) observed the whole sky in the period 1997 to 2001 using the two telescopes, one in Arizona and the other in Chile, in the J (1.25 μm), H (1.65 μm) and K_s (2.17 μm) bands. The survey cataloged 3×10^8 point like sources including YSOs.

Spitzer Space Telescope (SST) was launched with three instruments InfraRed Camera (IRAC), InfraRed Spectrograph (IRS), and Multiband Imaging Photometer for Spitzer (MIPS) in August 2003. These instruments cover the wavelength range from 3.6 μm to 160 μm. SST conducted several surveys, the Gould Belt Survey, the Galactic Legacy Infrared Mid-Plane Survery Extraordinaire (GLIMPSE), and “A 24 and 70 Micron Survey of the Inner Galactic Disk with MIPS" (MIPSGAL).

These surveys are useful for constructing the SED of YSOs. The far infrared emission was measured by the Herschel Space Observatory in the years from 2009 to 2913 although the survey was not conducted.

Catalogues made by the surveys serve for selection of sources for targeted observations. At the same time, the catalogues are used to census the population of each subcategory. The life time of each class is often derived from the population under the tacit assumptions that the birth rate is somehow constant and that all the YSOs follow more or less similar evolutionary paths.

4. Era of Imaging

As shown in the previous sections, the technological advances in observations have broadened our knowledge on the protoplanetary disks in these three decades. Very recent progress has been brought from the radio interferometer, ALMA. ALMA has improved angular resolution to sub arcsecond in the millimeter and sub-millimeter observations. At the same time, the image quality has been very much improved thanks to many antennas, currently fifty four 12 m ones and twelve 7 m ones. ALMA has been providing interesting topics in the study of star formation and protoplanetary disks. This section shows several topic interesting the author.

4.1 HD142527

HD142527 is a Herbig Fe star star surrounded by a transitional disk exhibiting a wide gap with a radial width of approximately 100 au. The transitional disk is highly asymmetric and looks like an arc when seen in 1.3 mm (Casassus et al. [11]) and 0.89 mm (Fukagawa et al. [12]) continuum. The northern part of the disk is very bright while the southern part is dark. The brightness contrast amounts to 60. Since the $\sim$ 1 mm emission is ascribed to relatively large ($\sim$ 1 mm) dust grains in the protoplanetary disk, the observations indicate that the dust grains are concentrated in both the radial and azimuthal directions.

Gas and perhaps small dust grains are distributed less asymmetrically in the transitional disk. Muto et al. [13] have evaluated the dust and gas distribution in the northern and southern parts of the disk based on the radiative equilibrium model which takes account of the absorption, scattering, and emission of radiation in the wavelength range of 0.1 μm to 3.16 mm by the dust having the power law size distribution with the maximum radius of 1 mm. The dusts are more concentrated in the northern disk than the gas. The gas is spread also in the radial direction. While the continuum emission has sharp inner and outer edges, the gas is distributed more broadly. The gas motion derived from the $C^{18}O$ (3-2) emission is consistent with the Keplerian rotation.

Soon et al. [14] have extended the analysis by Muto et al. [13] to all the azimuthal directions. They find that the emission from the north western disk cannot be reproduced as far as the conventional opacity model is applied. The conventional opacity model (i.e., the Mie theory) employs the assumption a dust grain is a sphere of a uniform dielectric constant (see, e.g., Draine [15]). When the dust radius is comparable to the photon wavelength, scattering dominates over the absorption by a factor of 10. The scattering reduces emergent radiative flux substantially when the effective optical depth is larger than unity (see, e.g, Rybicki and Lightman [16]). Soon et al. [14] pointed out a possibility that the real scattering opacity can be much smaller than the conventional value.

4.2 HL Tau

HL Tau was observed during the 2014 ALMA long baseline campaign in the wavelength bands, λ = 2.9, 1.3 and 0.87 mm [17]. The radio observation revealed that the protoplanetary disk consists of thin concentric multiple rings. In other words, the disk is geometrically thin and have many gaps of which origin is still unknown. The disk is highly symmetric in the azimuthal direction so that the inclination was precisely evaluated to be $46.^\circ72 \pm 0.^\circ05$.

HL Tau is an ideal target for modeling the protoplanetary disk since the disk is highly symmetric around the rotation axis. This means that we can argue the viewing angle dependent radiation from the disk and we can derive many constraints from the data. First the radio disk should be geometrically thin and flat otherwise the near side should be significantly different from the far side. This means that the protoplanetary disk consists of at least two components, the geometrically thin radio disk and the flared disk irradiating the near infrared. (See, e.g., Murakawa et al. [18] for the near infrared images of HL Tau.)

K. Mochida and I have constructed a multi-color model for the HL Tau disk with the above mentioned constraints in mind. The model image also suggests a possibility that the conventional opacity model may overestimate the scattering efficiency. Figure 1 shows our model intensity maps. The left half of each panel denotes the model image obtained with the conventional opacity model, while the right half does that obtained with the model opacity in which the scattering opacity is reduced artificially by a factor of 10. The scattering opacity is by a factor of 10 larger than the absorption opacity at $\lambda = 0.87$ mm in the conventional opacity model.

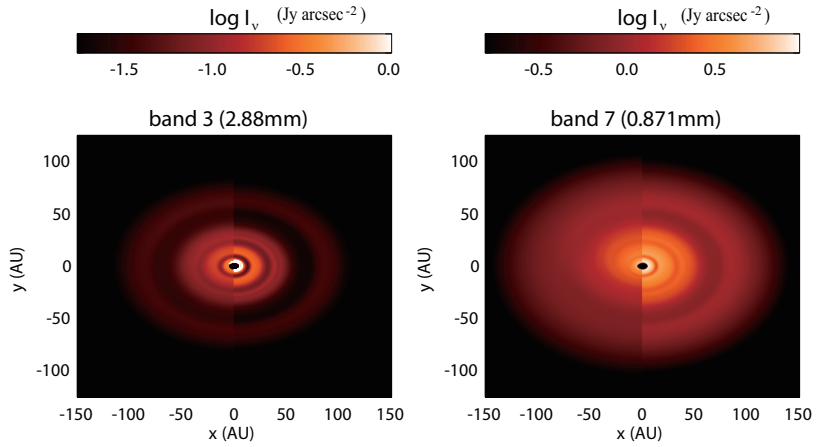

Figure 1: Model intensity maps for HL Tau. The left and right panels denote the intensity distributions at 2.88 and 0.87 mm, respectively. The left half of each panel shows the intensity for the model in which the conventional model opacity is employed. The right half of each panel shows that for model in which the scattering opacity is artificially reduced by a factor of 10.

The large scattering opacity affects the model image seriously. First the dark rings are obscured. Second the peak brightness is reduced, i.e., the intensity is much lower than the blackbody one although the disk is optically thick. Both of them contradict with the observed intensity maps. The dark rings are clear and the SED is close to the blackbody one in the region of a few tens au

from the central star in the observation. We need to reconsider the validity of the conventional dust model opacity.

4.3 L1551 NE

L1551 NE is binary of which components are protostars. Takakuwa et al. [19] observed the circumbinary disk with ALMA in 0.9 mm continuum, $C^{18}O$ (3-2), and ^{13}CO (3-2) lines. The circumbinary disk shows two opposing bright U-shaped features in the 0.9 mm continuum map. circumbinary disk. The molecular lines trace non-axisymmetric deviation from the Keplerian rotation there. These observed features are explained by spiral arms induced by the gravitational torques of the binary. By using a numerical simulation, they have confirmed that the gravitational torque produces surface density enhancement through spiral shock waves in the location of the U-shaped features. The deviation from the Keplerian rotation coincides with the inward motion due to the angular momentum loss by the shock waves in the simulation. Both the continuum and lines coincide with the simulation.

The good agreement between the observation and simulation indicates that gravitational torques of the binary constitute the primary driver for exchanging angular momentum so as to permit infall through the circimbinray disk of L1551 NE. It is interesting to observe the binary in higher spatial resolution since the observation was performed in November 2012 and the resolution then was lower. Higher spatial resolution will show the circumstellar disks clearly.[1]

4.4 L1527

An important question, in which phase a newly born star has its protoplanetary disk, may be still controversial. It is partly because still some recent numerical simulations suffer from insufficient resolution and/or lack of important physical processes (see, e.g., Machida et al. [20]).

A clue for the question may come from observations of a low mass protostar embedded in a protostellar core, L1527. Sakai et al. [21] observed infalling envelope and rotating disk around the protostar with ALMA. They found a sharp transition in chemistry and kinematics around 100 au from the protostar. A rotating-infalling rotating envelope is traced with emission from cyclic-C_3H_2 in the region beyond 100 au. On the other hand the SO line emission shows a compact single-peaked emission centered at the protostar. This indicates that the disk outer boundary is located at 100 au in this object.

Sakai et al. [21] argue that the transition takes place not at the centrifugal radius but at the centrifugal barrier. Here the centrifugal radius means the radius at which the centrifugal force is balanced with the gravity. The radius of the centrifugal barrier is a half of the centrifugal radius. They argue that a gas element reaches once the centrifugal barrier if it accretes from a distant place without loosing its energy and angular momentum. The gravitational potential is approximated by that of a point mass in their argument. Then the radial velocity is evaluated to be

$$v_r = \pm\sqrt{\frac{2GM}{r} - \left(\frac{\ell}{r}\right)^2} = \pm\sqrt{\frac{GM}{r_c}}\left[\frac{2r_c}{r} - \left(\frac{r_c}{r}\right)^2\right]^{1/2}, \tag{4.1}$$

$$r_c = \frac{\ell^2}{GM}, \tag{4.2}$$

[1] A follow-up observation by Takakuwa et al. arXiv1702.05562 will appear in ApJ.

where ℓ and r_c denote the specific angular momentum of the gas element and the centrifugal radius, respectively. Equation (4.1) indicates that the gas element reaches $r = r_c/2$ once and then flows back to the centrifugal radius. Eq. (4.1) fits with their data. Similar kinematics are observed by Ohashi et al. [22] and Sakai et al. [24], although the former shows a different interpretation. Another object showing similar kinematics is found by Oya et al. [23].

The model of Sakai et al. [21] do not take account of fluid effects. However, a gas element will be decelerated by pre-existing disk or another gas element accreting earlier and now flowing outwards. Do the gas elements reach the centrifugal barrier continuously? One possibility is shown in Figure 2. The panels show the 2D simulation of an accreting young star. The protoplanetary disk is assumed to be geometrically thin and the infalling envelope is thick. Each panel shows a snap shot at the time indicated on the top of the diagram. The inflow and outflow coexist vertically. The simulation suggests heating by shock, which may induce chemical change around the centrifugal barrier.

5. Short Summary

Thanks to the great advances in the observations our knowledge on the protoplanetary disks have been very much broadened. We have much observational data and constraint for many objects. They are useful for constructing models for each object. However this does not mean that all the basic questions have been resolved. Even the earliest stage of the protoplanetary disk is currently discussed (see §4). Also the evolutionary path has not been fixed. Highly non-axisymmetric features are still mysterious and the formation mechanism is not settled. It should be also noted that only outer part of the protoplanetary disks are spatially resolved. The current highest spatial resolution is of the order of 10 au for the nearby star forming regions. We still need theoretical modeling for structure of the inner disk.

The author thanks K. Mochida for his contribution to the numerical modeling of HL Tau. This manuscript owes to discussions with the collaborators of the author on the objects discussed in §4. He also thanks the LOC of ACPS 2016 for their warm hospitality during his stay in St. Petersburg. This work was supported in part by MEXT KAKENHI Grant Number 26103702 and JSPS KAKENHI Grant Number JP15K05017.

References

[1] C.J. Lada, *Star formation - From OB associations to protostars* in proceedings of *the IAU Symposium No. 115, Star Forming Regions*, D. Reidel (1987) 1

[2] C.J. Lada, B. Wilking, *The nature of the embedded population in the Rho Ophiuchi dark cloud - Mid-infrared observations*, *ApJ* 287 (1984) 610

[3] P. André, D. Ward-Thompson, Barsony, M. *Submillimeter continuum observations of Rho Ophiuchi A - The candidate protostar VLA 1623 and prestellar clumps*, *ApJ* 406 (1993) 122

[4] J.P. Williams, L.A. Cieza, *Protoplanetary Disks and Their Evolution*, *Ann. Rev. Astron. Astrophys.* 49 (2011) 67

[5] A. Dutrey, S. Guilloteau, M. Simon, *Images of the GG Tau rotating ring*, *A&Ap.* 286 (1994) 149

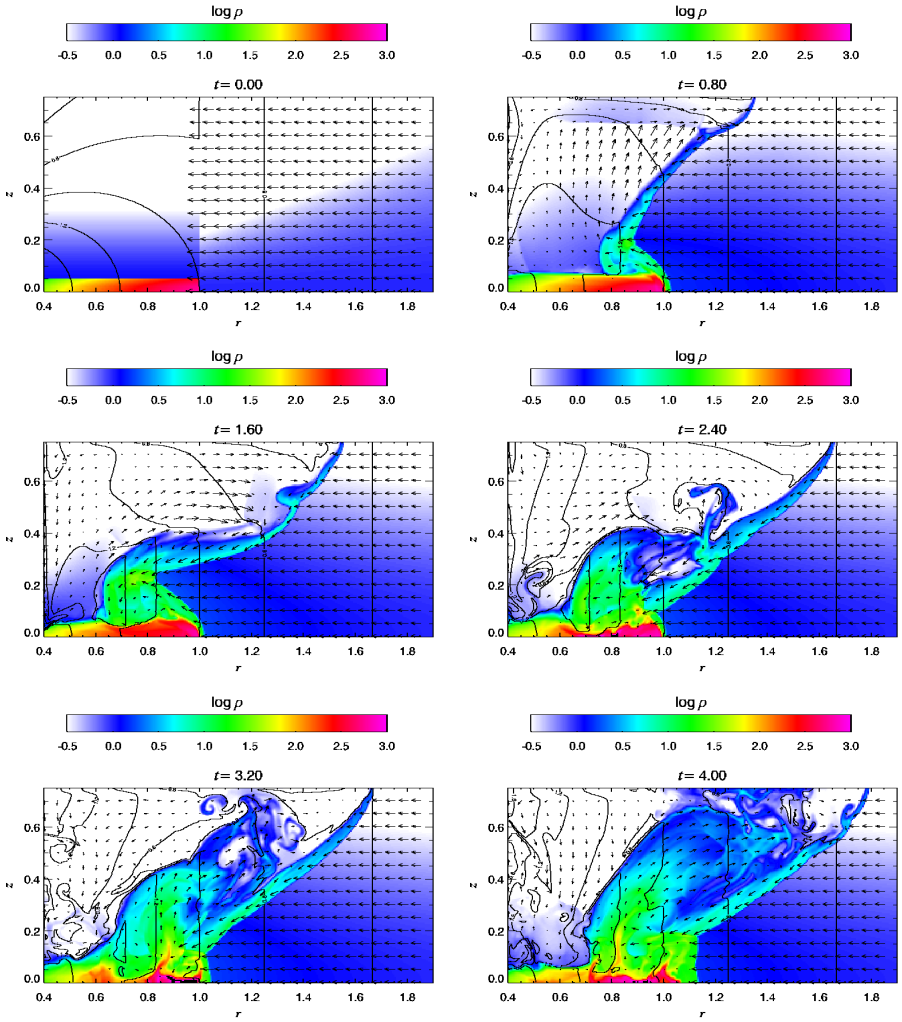

Figure 2: 2D axisymmetric simulation for dynamical accretion onto protostar with a disk. Each panel denotes the density distribution by color, the rotation velocity by contour, and (v_r, v_z) by arrows. The top left denotes the initial condition. This simulation is performed in a non-dimensional unit.

[6] Y.-W. Tang, A. Dutrey, S. Guilloteau et al. *Mapping CO Gas in the GG Tauri A Triple System with 50 au Spatial Resolution*, *ApJ* 820 (2016) 19

[7] C. R. O'Dell, Z. Wen, X. Hu *Discovery of new objects in the Orion nebula on HST images - Shocks, compact sources, and protoplanetary disks*, *ApJ* 410 (1993) 696

[8] C. R. O'Dell, Z. Wen, *Postrefurbishment mission Hubble Space Telescope images of the core of the Orion Nebula: Proplyds, Herbig-Haro objects, and measurements of a circumstellar disk*, *ApJ* 436 (1994) 194

[9] D.L. Padgett, W. Brandner, K.R. Stapelfeldt, S.E. Strom, S. Tereby, D. Koerner, *HUBBLE SPACE TELESCOPE/NICMOS Imaging of Disks and Envelopes around Very Young Stars*, *ApJ* 117 (1999) 1490

[10] T. Montmerle, L. Koch-Miramond, E. Falgarone, J.E. Grindlay, *EINSTEIN Observations of the Rho Ophiuchi Dark Cloud: an X-ray Christmas Tree ApJ* 269 (1983) 182

[11] S. Casassus, G. van der Plas, S. Perez M, et al., *Flows of gas through a protoplanetary gap*, *Nature* 493 (2013) 191

[12] M. Fukagawa, T. Tsukagoshi, M. Momose et al., *Local Enhancement of the Surface Density in the Protoplanetary Ring Surrounding HD 142527*, *PASJ* 65 (2013) L14

[13] T. Muto, T. Tsukagoshi, M. Momose et al. *Significant gas-to-dust ratio asymmetry and variation in the disk of HD 142527 and the indication of gas depletion*, *PASJ* 67 (2015) 122

[14] K.-L. Soon, T. Hanawa, T. Muto, T. Tsukagoshi, M. Momose, *Detailed modeling of dust distribution in the disk of HD 142527*, *PASJ* 69 (2017) 34

[15] B.T. Draine, *Physics of the Interstellar and Intergalactic Medium*, Princeton Univ. (2011) Chap. 22

[16] G.B. Rybicki, A.P. Lightman, *Radiative Processes in Astrophysics*, Wiley (1979) p. 33

[17] A. Partnership, C.L. Brogan, L.M. Pérez et al. *The 2014 ALMA Long Baseline Campaign: First Results from High Angular Resolution Observations toward the HL Tau Region*, *ApJ* 808 (2015) 3

[18] K. Murakawa, S. Oya, T.-S. Pyo, M. Ishii, *Near-infrared multiwavelength imaging polarimetry of the low-mass proto-stellar object HL Tauri*, *A&Ap* 492 (2008) 731

[19] S. Takakuwa, M. Saito, K. Saigo, T. Matsumoto, J. Lim, T. Hanawa, P.T.P. Ho, *Angular Momentum Exchange by Gravitational Torques and Infall in the Circumbinary Disk of the Protostellar System L1551 NE*, *ApJ* 796 (2014) 1

[20] M. Machida, S. Inutsuka, T. Matsumoto, *Conditions for circumstellar disc formation: effects of initial cloud configuration and sink treatment*, *MNRaS* 438 (2014) 2278

[21] N. Sakai, T. Sakai, T. Hirota, *Change in the chemical composition of infalling gas forming a disk around a protostar*, *Nature* 507 (2014) 78

[22] N. Ohashi, K. Saigo, Y. Aso et al., *Formation of a Keplerian Disk in the Infalling Envelope around L1527 IRS: Transformation from Infalling Motions to Kepler Motions*, *ApJ* 796 (2014) 131

[23] Y. Oya, N. Sakai, A, López-Sepulcre et al., *Infalling-Rotating Motion and Associated Chemical Change in the Envelope of IRAS 16293-2422 Source A Studied with ALMA*, *ApJ* 824 (2016) 88

[24] N. Sakai, Y. Oya, A. López-Sepulcre et al., *Subarcsecond Analysis of the Infalling-Rotating Envelope around the Class I Protostar IRAS 04365+2535*, *ApJ* 820 (2016) 34